



Structural insights into sphingosine-1-phosphate receptor activation

Leiye Yu^{a,b,c,1}, Licong He^{d,1}, Bing Gan^{a,1}, Rujuan Ti^{e,1}, Qingjie Xiao^f, Xin Yang^{g,2}, Hongli Hu^a, Lizhe Zhu^{e,2}, Sheng Wang^{d,2}, and Ruobing Ren^{a,b,2}

Edited by Ping Yin, Huazhong Agriculture University, Wuhan, China; received September 27, 2021; accepted February 22, 2022 by Editorial Board Member Nieng Yan

As a critical sphingolipid metabolite, sphingosine-1-phosphate (S1P) plays an essential role in immune and vascular systems. There are five S1P receptors, designated as S1PR1 to S1PR5, encoded in the human genome, and their activities are governed by endogenous S1P, lipid-like S1P mimics, or nonlipid-like therapeutic molecules. Among S1PRs, S1PR1 stands out due to its nonredundant functions, such as the egress of T and B cells from the thymus and secondary lymphoid tissues, making it a potential therapeutic target. However, the structural basis of S1PR1 activation and regulation by various agonists remains unclear. Here, we report four atomic resolution cryo-electron microscopy (cryo-EM) structures of G_i-coupled human S1PR1 complexes: bound to endogenous agonist d18:1 S1P, benchmark lipid-like S1P mimic phosphorylated Fingolimod [(S)-FTY720-P], or nonlipid-like therapeutic molecule CBP-307 in two binding modes. Our results revealed the similarities and differences of activation of S1PR1 through distinct ligands binding to the amphiphilic orthosteric pocket. We also proposed a two-step “shallow to deep” transition process of CBP-307 for S1PR1 activation. Both binding modes of CBP-307 could activate S1PR1, but from shallow to deep transition may trigger the rotation of the N-terminal helix of G_{αi} and further stabilize the complex by increasing the G_{αi} interaction with the cell membrane. We combine with extensive biochemical analysis and molecular dynamic simulations to suggest key steps of S1P binding and receptor activation. The above results decipher the common feature of the S1PR1 agonist recognition and activation mechanism and will firmly promote the development of therapeutics targeting S1PRs.

sphingosine-1-phosphate | S1P receptor | active state structure

Sphingolipids, named after the sphinx in Egypt to represent its mysterious role, include sphingosine-1-phosphate (S1P), sphingosine, ceramide, and other complex sphingolipids, like glycosphingolipids and sphingomyelins (1–3). S1P, acting as a bioactive lipid mediator, is mainly derived from the deacylation of ceramide or interconverted with sphingosine and secreted by vascular endothelial cells to the circulation predominantly (4–7). Intracellular S1P promotes cellular proliferation (8) and close links to a myriad of essential cellular processes, including immune-cell trafficking (9), angiogenesis (10, 11), and vascular maturation (12). Plasma S1P helps maintain vascular integrity and regulate vascular leaks (13). Besides, S1P is identified as an early risk factor of lung cancer (14) and a crucial mediator of cardioprotection (15, 16). Thus, abnormal S1P production leads to the occurrence and progression of numerous severe diseases, such as metabolic syndrome, cancers, autoimmune disorders such as multiple sclerosis (MS), and kidney and cardiovascular diseases (7, 17–20).

Currently, the therapeutic molecules targeting S1P receptors (S1PRs) can be divided into two classes: the lipid-like S1P mimics, such as (S)-FTY720-P (21), or the nonlipid-like molecules, such as clinical drugs BAF-312 (siponimod) (22), RPC-1063 (ozanimod) (23), and CBP-307, which is still in clinical trials (Fig. 1A). (S)-FTY720-P is the *in vivo* phosphorylated product of Fingolimod to treat relapsing MS (3, 24). Siponimod and ozanimod were also launched to treat relapsing MS or ulcerative colitis in recent years (25, 26). Despite the broad indications and urgent need, the development of therapeutics is primarily limited by the high sequence similarity of S1PRs and less-characterized functions of S1PR2 to S1PR5. The inactive structure of S1PR1 bound with an antagonist was reported in 2012 (27). Recently, the crystal structure of active S1PR3 bound to Fab and endogenous agonist S1P and active-state structures of S1PR1,3,5 bound to the G_i complex and different agonists were reported (28–30). Here, we report four atomic resolution cryo-electron microscopy (cryo-EM) structures of G_i-coupled human S1PR1 complexes bound to d18:1 S1P, (S)-FTY720-P, or CBP-307 in two binding modes. This structural information further supplements the

Significance

Sphingosine-1-phosphate (S1P) receptors are valid therapeutic targets to treat autoimmune diseases, such as relapsing multiple sclerosis and ulcerative colitis. Particularly, S1PR1 is well characterized because of its nonredundant functions on T and B cells' egress. However, the activation mechanism of S1PR1 is still poorly understood. Therefore, we determined active S1PR1–G_i complex structures bound to distinct agonists. Phosphorylated Fingolimod [(S)-FTY720-P] could modulate lymphocyte trafficking and treat multiple sclerosis. The nonlipid-like agonist CBP-307 is currently being evaluated in a global phase 2 clinical study in moderate to severe ulcerative colitis and Crohn's disease. Meanwhile, two binding poses of CBP-307 and the unoccupied subpocket we observed may provide opportunities to improve further the efficacy and specificity of CBP-307 targeting different S1P receptors.

Author contributions: L.Z., S.W., and R.R. designed research; L.Y., L.H., B.G., R.T., and Q.X. performed research; H.H., L.Z., and R.R. analyzed data; X.Y. contributed new reagents and analyzed data; and R.R. wrote the paper.

The authors declare no competing interest.

This article is a PNAS Direct Submission. P.Y. is a guest editor invited by the Editorial Board.

Copyright © 2022 the Author(s). Published by PNAS. This open access article is distributed under Creative Commons Attribution-NonCommercial-NoDerivatives License 4.0 (CC BY-NC-ND).

¹L.Y., L.H., B.G., and R.T. contributed equally to this work.

²To whom correspondence may be addressed. Email: renruobing@cuhk.edu.cn, wangsheng@sibcb.ac.cn, zhulizhe@cuhk.edu.cn, or xyang@connectpharm.com.

This article contains supporting information online at <http://www.pnas.org/lookup/suppl/doi:10.1073/pnas.2117716119/-DCSupplemental>.

Published April 11, 2022.

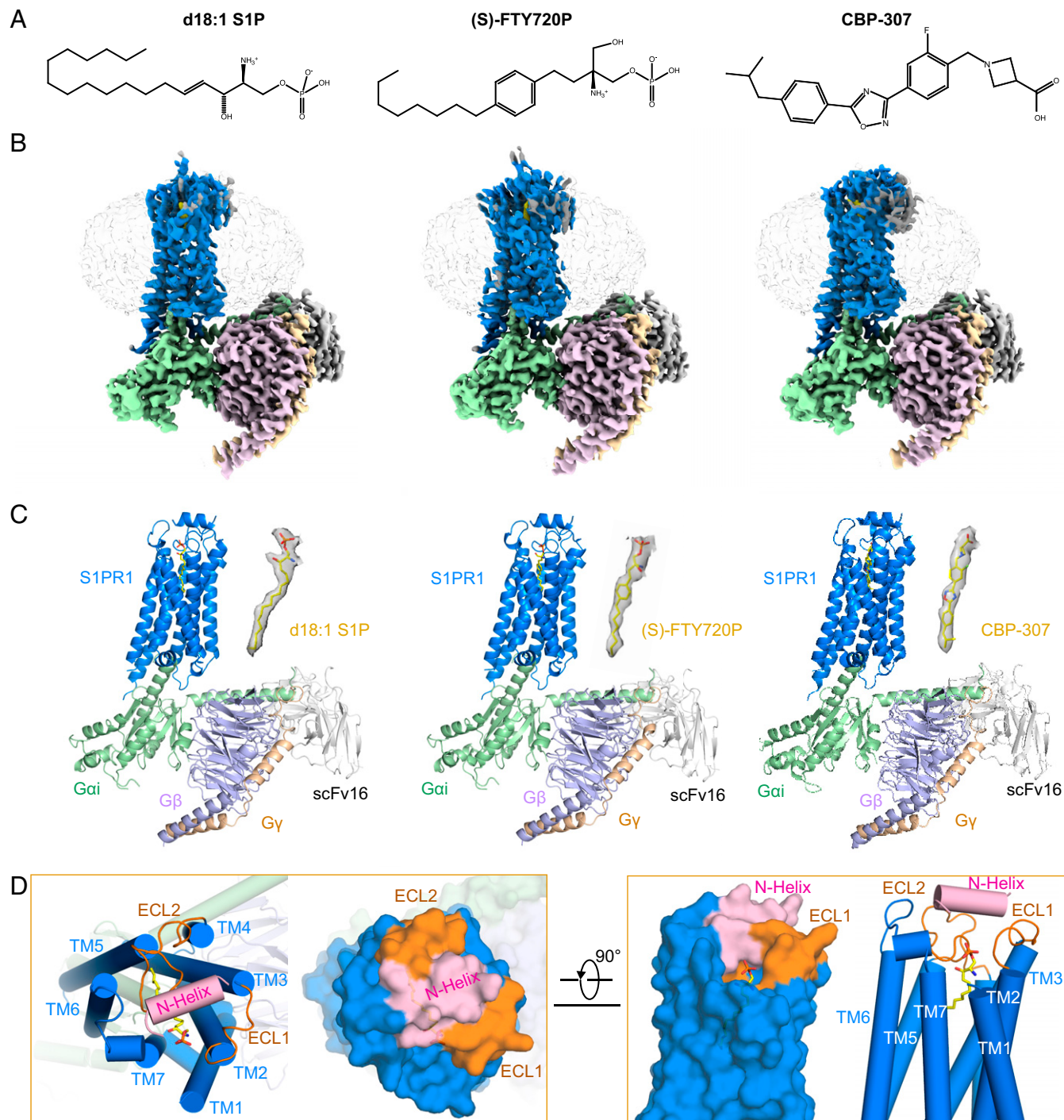


Fig. 1. Cryo-EM maps and structures of human S1PR1 with G_i and agonist d18:1 S1P, (S)-FTY720-P, or CBP-307. (A) Structural formulas of three agonists: d18:1 S1P, (S)-FTY720-P, and CBP-307. (B) Cryo-EM maps of human S1PR1 with G_i and agonist d18:1 S1P, (S)-FTY720-P, or CBP-307. The densities of S1PR1, $G_{\alpha i1}$, G_{β} , G_{γ} , and scFv16 are shown in marine, pale green, pink, wheat, and gray, respectively. (C) Structural models of human S1PR1 with G_i , scFv16, and agonist d18:1 S1P (PDB ID code 7VIE), (S)-FTY720-P (PDB ID code 7VIF), or CBP-307 (PDB ID code 7VIG). S1PR1, $G_{\alpha i1}$, G_{β} , G_{γ} , and scFv16 are shown in marine, pale green, light blue, wheat, and gray, respectively. Ligands in density (yellow) are shown on the right side of the models. (D) The extracellular lid of S1PR1 is shown in the top and side views (surface and cartoon modes). N-helix, ECL1/2, and TM helices are pink, orange, and marine, respectively.

binding details of different agonists and explores the activation mechanism of S1PR1, which will firmly promote the development of therapeutics targeting S1PRs.

Results

S1PR1- G_i Complexes Assembling and Overall Structures. For structure-determination purposes, we engineered the human S1PR1 with an N-terminal apocytochrome b562 (BRIL) fusion

and the addition of affinity tags (an N-terminal FLAG tag and a C-terminal 10X His tag) (SI Appendix, Fig. S1A). S1PR1, $G_{\alpha i1}$, G_{β} , and $G_{\gamma 2}$ were coexpressed in *Sf9* insect cells using baculovirus to form the S1PR1- G_i complex. Agonist d18:1 S1P, (S)-FTY720-P, or CBP307 and the antibody fragment scFv16 were added during purification to enable a stable complex formation. The cell membrane was solubilized in lauryl maltose neopentyl glycol and cholesteryl hemisuccinate and then purified by two steps using FLAG and nickel-affinity

beads sequentially. The concentrated samples were applied in size-exclusion chromatography to yield a monodisperse complex that contained all the components (*SI Appendix, Fig. S1B*).

The vitrified complexes were imaged by using a Titan Krios cryo-electron microscope. Images were processed to yield a final map at an overall resolution of 2.86 Å for d18:1 S1P-bound (Protein Data Bank [PDB] ID code 7VIE), of 2.83 Å for (S)-FTY720-P-bound (PDB ID code 7VIF), and of 2.98 Å and 2.89 Å for CBP-307-bound shallow (PDB ID code 7VIH) and deep (PDB ID code 7VIG) binding modes, respectively (Fig. 1*B* and *SI Appendix, Figs. S2–S5*). The densities for the N terminus and transmembrane (TM) helices of receptor and G-protein complexes were unambiguously determined, based on the well-traced α -helices and aromatic side chains (*SI Appendix, Figs. S2–S5*). Due to the flexibility, the N-terminal BRIL fusion, part of the extracellular loops, and long C-terminal residues are invisible. It is worth mentioning that the densities of agonists are also well defined (Fig. 1*C*).

S1PR1, with different agonists bound at the extracellular side and G_i complex bound at the intracellular side, demonstrates an active-state supercomplex, which is reminiscent of the structures of other G_i-coupled class A G protein-coupled receptors (GPCRs) (29, 31). The structural analysis reflects some common features for other lipid receptors, such as cannabinoid receptors (32) and CRTH2 (33). The extracellular loops (ECL1 to ECL2) and the N-terminal “cap” region are coordinated to exclude agonists from the extracellular solvent (Fig. 1*D, Left*). Besides, there is a cleft between TM1 and TM7 facing the membrane bilayer (Fig. 1*D, Right*). These observations suggest a common mechanism that these lipidic molecules, such as S1P, cannabinoid, and prostaglandins, may first integrate into the lipid bilayer before binding to the receptors.

Structures of d18:1 S1P and (S)-FTY720-P Binding Modes. Due to the structure similarity, d18:1 S1P and (S)-FTY720-P demonstrate almost identical fully extended conformations and form equivalent contacts in the orthosteric binding pocket of S1PR1 (Fig. 2*A* and *B*). The orthosteric pocket of S1PR1, which is highly conserved among all S1PRs (Fig. 2*A, left*, and *SI Appendix, Fig. S6*), is divided by a polar region on the top (composed by an N-terminal cap, ECL1, and ECL2) and a deep hydrophobic cavity (composed by TM3 and TM5 to TM7). These characters fit the zwitterionic nature of d18:1 S1P and (S)-FTY720-P well (Fig. 2*A* and *B*). Residues K34 and G106 form hydrogen bonds with the phosphate group of d18:1 S1P directly, while N101^{2,60} and S105 coordinate the amino group of d18:1 S1P (Fig. 2*C*). In addition, Y29 and R120^{3,28} may interact with the polar group of d18:1 S1P by van der Waals interactions, electrostatic interaction, or possible indirect interactions, such as water-mediated hydrogen bonds (*SI Appendix, Fig. S7A*). The interactions between the polar region of (S)-FTY720-P and S1PR1 also involve residues mentioned above. The three slight differences are: 1) Y29, but not K34, forms a hydrogen bond with the phosphate group of (S)-FTY720-P; 2) N101^{2,60} interacts with the hydroxymethyl group of (S)-FTY720-P, which does not exist in d18:1 S1P; and 3) S105 does not interact with (S)-FTY720-P directly (Fig. 2*C* and *SI Appendix, Fig. S7B*). Notably, the key residue E121^{3,29}, which interacts with ML056 in the S1PR1 inactive structure, also forms a hydrogen bond with the amino group of (S)-FTY720-P (Fig. 2*D*). In contrast, E121^{3,29} does not directly interact with the polar head of d18:1 S1P. It may interact with d18:1 S1P by van der Waals interactions and possible indirect interactions, such as water-mediated hydrogen bonds,

or stabilize the local conformation of the binding pocket through the hydrogen-bond network with surrounding residues (*SI Appendix, Fig. S7A*). To demonstrate the importance of these residues, we conducted the G_i dissociation assay for S1PR1 mutants. The results clearly showed that N101^{2,60}A, R120^{3,28}A, and E121^{3,29}A aborted G_i coupling significantly for both d18:1 S1P and (S)-FTY720-P (Fig. 2*E* and *F*). Y29A and K34A compromised the potency of d18:1 S1P by more than 30-fold, compared to two-fold for (S)-FTY720-P compared to wild-type S1PR1 (Fig. 2*E* and *F* and *SI Appendix, Table S2*). Our results suggested that hydrophilic residues on top of the pocket of S1PR1 play an essential role in stabilizing the polar head of d18:1 S1P and activating downstream G_i signaling.

The acyl chains of d18:1 S1P and (S)-FTY720-P are surrounded by numbers of hydrophobic residues, such as M124^{3,32}, F125^{3,33}, L128^{3,36}, S129^{3,37}, L195, F210^{5,47}, W269^{6,48}, L272^{6,51}, L276^{6,55}, and L297^{7,39} on TM3 and TM5 to TM7 (*SI Appendix, Fig. S7C*). The superposition of d18:1 S1P-bound and (S)-FTY720-P-bound S1PR1 structures showed that acyl chains of d18:1 S1P extend deeper than the tail of (S)-FTY720-P (*SI Appendix, Fig. S7C*). We also examined the effects of these hydrophobic residues on agonist binding and G_i activation. Unsurprisingly, the potency of d18:1 S1P and (S)-FTY720-P to most of the S1PR1 mutants was decreased (*SI Appendix, Table S2*). W269^{6,48}, L272^{6,51}A, L276^{6,55}A, and L297^{7,39}A showed the most significant changes (*SI Appendix, Fig. S7D* and *E*). Together, these interactions make a high binding affinity for d18:1 S1P and (S)-FTY720-P to S1PR1. It is worth mentioning that the signature residues for GPCR activation, F210^{5,47} and W269^{6,48}, are located on the bottom of the pocket, indicating the critical role of the S1P acyl chain for S1PR1 activation.

Activation Mechanism of S1PRs. We firmly believe that, together with the antagonist ML056-bound inactive S1PR1 structure (27) and the active S1PR1 structures bound to G_i and various agonists, it is a proper prototype to propose the activation mechanism of S1PRs. Here, we used d18:1 S1P-bound structure as the representative active state to analyze the conformational changes during the S1PR1 activation process. In the superposition of active and inactive S1PR1 structures, the overall rmsd is 1.222 Å over 269 residues majorly located on the TM region. The extracellular half of S1PR1 showed an unapparent change that the N terminus of TM1 moved toward TM7 by 2.7 Å (C_{α} of Val50 as reference). In contrast, the conformation of intracellular half significantly changed with TM6 moving away from TM7 by 8.3 Å (C_{α} of Lys250 as reference) and TM7 swinging inward by 3.4 Å (C_{α} of Leu313 as reference), resulting in the G_{ai} coupling (Fig. 3*A*).

Further careful examinations of signature residues in the orthosteric pocket of S1PR1 showed a well-organized spatial rearrangement of a few side chains. The most attractive residue is F210^{5,47}, located at the bottom of the pocket. In the inactive structure, F210^{5,47} points to TM3, but does not interact with ML056. However, upon d18:1 S1P binding, F210^{5,47} rotates about 130° to avoid a stereo clash with the acyl chain of d18:1 S1P inserted deeper than ML056. Then, the F210^{5,47} rotation results in the rotation of F273^{6,52} and pushes TM6 moving outward. L128^{3,36} also rotates away from W269^{6,48} to adapt to the accommodation of d18:1 S1P and weaken the interactions between TM3 and TM6. It will facilitate the activation of S1PR1 (Fig. 3*B*). A similar observation is in the (S)-FTY720-P-bound structure (Fig. 3*C*). Thus, the initiation of S1PR1 activation is triggered most likely by touching L128^{3,36} and

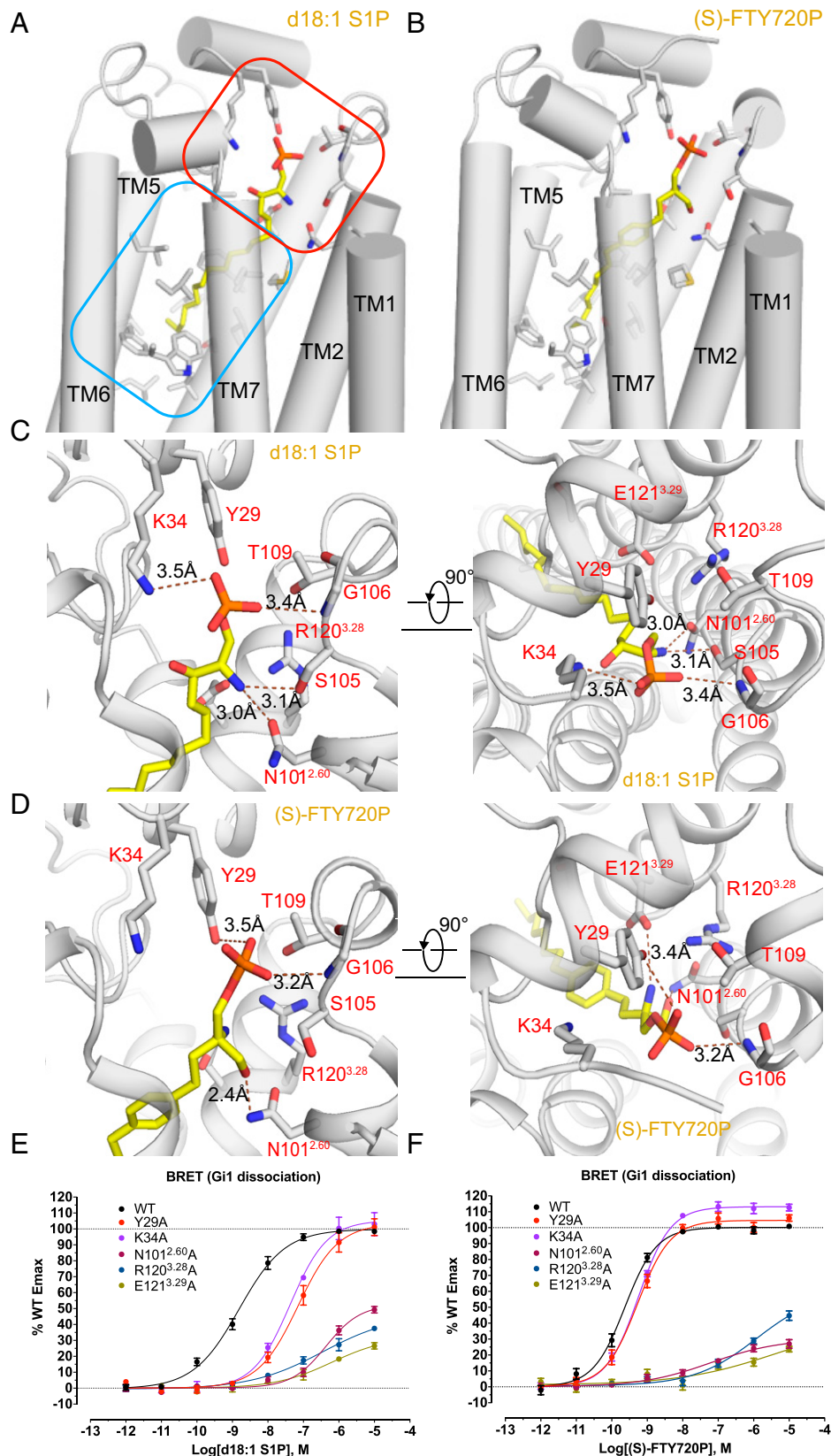


Fig. 2. Orthosteric binding pockets of d18:1 S1P and (S)-FTY720-P in S1PR1. (A) The binding pocket of d18:1 S1P in S1PR1. d18:1 S1P is shown in yellow. S1PR1 is gray with residues surrounding the binding pocket shown in sticks. The head and tail parts of the binding pocket are indicated by red and blue rectangular frames, respectively. (B) The similar binding pocket of (S)-FTY720-P in S1PR1 compared to d18:1 S1P. (S)-FTY720-P and S1PR1 are shown in the same color as in A. (C) The key residues, including K34, N101^{2.60}, S105, and G106, interact with the head group of d18:1 S1P. Side and top views are shown. The polar interactions are shown with dashed lines and indicated distances. (D) The key residues, including Y29, N101^{2.60}, G106, and E121^{3.29}, interact with the head group of (S)-FTY720-P and are shown in the same color as in C. (E) The effects of mutants Y29A, K34A, N101^{2.60}A, R120^{3.28}A, and E121^{3.29}A of S1PR1 on d18:1 S1P induced G_i signal activation measured by G_i dissociation assay (BRET assay). All data are mean ± SEM of three independent experiments for wild type or mutants. (F) The effects of mutants Y29A, K34A, N101^{2.60}A, R120^{3.28}A, and E121^{3.29}A of S1PR1 on (S)-FTY720-P-induced G_i signal activation measured by G_i dissociation assay (BRET assay). All data are mean ± SEM of three independent experiments for wild type or mutants.

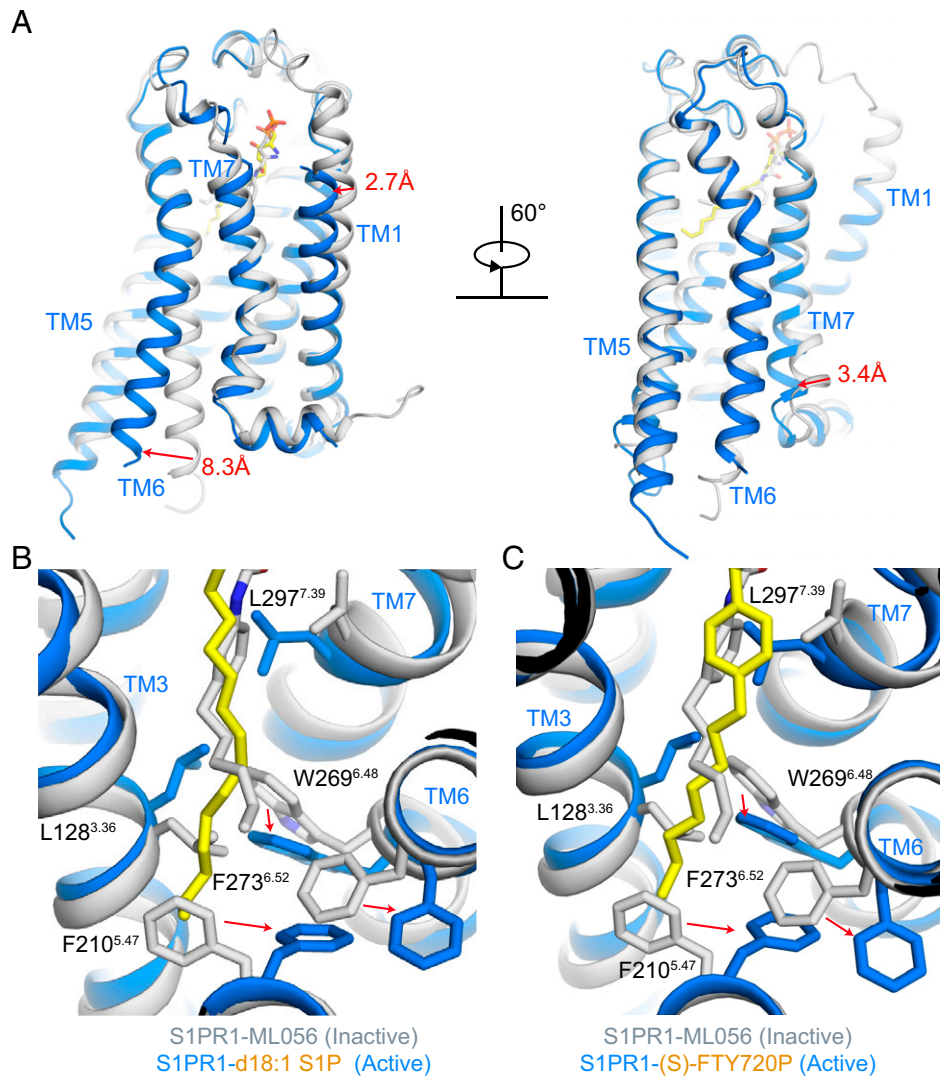


Fig. 3. Conformational changes between active and inactive forms of S1PR1. (A) TM helix shifts between S1PR1 (colored in marine) in the active form of the S1PR1-G_i-d18:1 S1P complex (PDB ID code 7VIE) and S1PR1 (colored in gray) in the inactive form of the S1PR1-ML056 complex (PDB ID code 3V2Y). Red arrows indicate significant shifts of TM1, TM6, and TM7 with distances. (B) Conformational changes of key residues at the bottom of the pockets between active (d18:1 S1P-bound) and inactive forms are shown in marine and white. d18:1 S1P and ML056 are shown in yellow and white, respectively. Red arrows indicate the directions of conformational changes of L128^{3.36}, F210^{5.47}, W269^{6.48}, F273^{6.52}, and L297^{7.39}, which are shown in sticks. The directions of conformational changes of F210^{5.47}, W269^{6.48}, and F273^{6.52}. (C) Conformational changes of key residues at the bottom of the pocket between active [(S)-FTY720-P-bound] and inactive forms are shown in marine and white. (S)-FTY720-P and ML056 are shown in yellow and white, respectively. Residues of L128^{3.36}, F210^{5.47}, W269^{6.48}, F273^{6.52}, and L297^{7.39} are shown in sticks. Red arrows indicate the conformational changes of F210^{5.47}, W269^{6.48}, and F273^{6.52}.

F210^{5.47} upon agonist binding. The slight conformational change of the extracellular half of TM7 is due to the movement of L297^{7.39} to form hydrophobic interaction with the acyl chain of d18:1 S1P and (S)-FTY720-P (Fig. 3 B and C).

Structures of CBP-307 Binding Modes. CBP-307 is a synthetic nonlipid-like molecule targeting S1PR1/4/5 specifically. In the process of structure determination, there are two classes of particles with comparable map quality showing slight differences by hetero refinement (*SI Appendix*, Fig. S4A). After carefully checking the densities of the receptor, G_i, and CBP-307, we found that CBP-307 adopted two distinct binding modes (Fig. 4A). Then, two structural models were built and superimposed to analyze the structural differences. Only the receptor was used for alignment, and the overall rmsd is 0.313 Å over 257 residues, indicating the identical conformation of S1PR1 in these two binding modes. We used “shallow” and “deep” to define these two binding modes because CBP-307 in the deep mode is inserted 1.5 Å deeper into the pocket than that in the

shallow mode (Fig. 4B). Densities of CBP-307 in these two structures are shown (Fig. 4C).

Similar to d18:1 S1P and (S)-FTY720-P structures, residues Y29, K34, N101^{2.60}, G106, R120^{3.28}, and E121^{3.29} form a hydrophilic pocket to coordinate the carboxyl group of CBP-307. The functional mutagenesis data also suggested the importance of these polar residues (Fig. 4D and *SI Appendix*, Table S2). For hydrophobic residues, the G_i dissociation assay showed that W269^{6.48}A, L272^{6.51}A, and L276^{6.55}A weakened CBP-307-mediated G_i signal, similar to d18:1 S1P (*SI Appendix*, Fig. S8 and Table S2). Notably, F125A also weakened the CBP-307-mediated G_i signal significantly, indicating its potential role in interacting with the benzene ring of CBP-307 (*SI Appendix*, Fig. S8 and Table S2).

After carefully comparing the detailed interactions between CBP-307 and S1PR1 in two binding modes, we noticed that the surrounding residues that interacted with CBP-307 in two structures were significantly different. In the shallow mode, the carboxyl group of CBP-307 forms a hydrogen bond to K34,

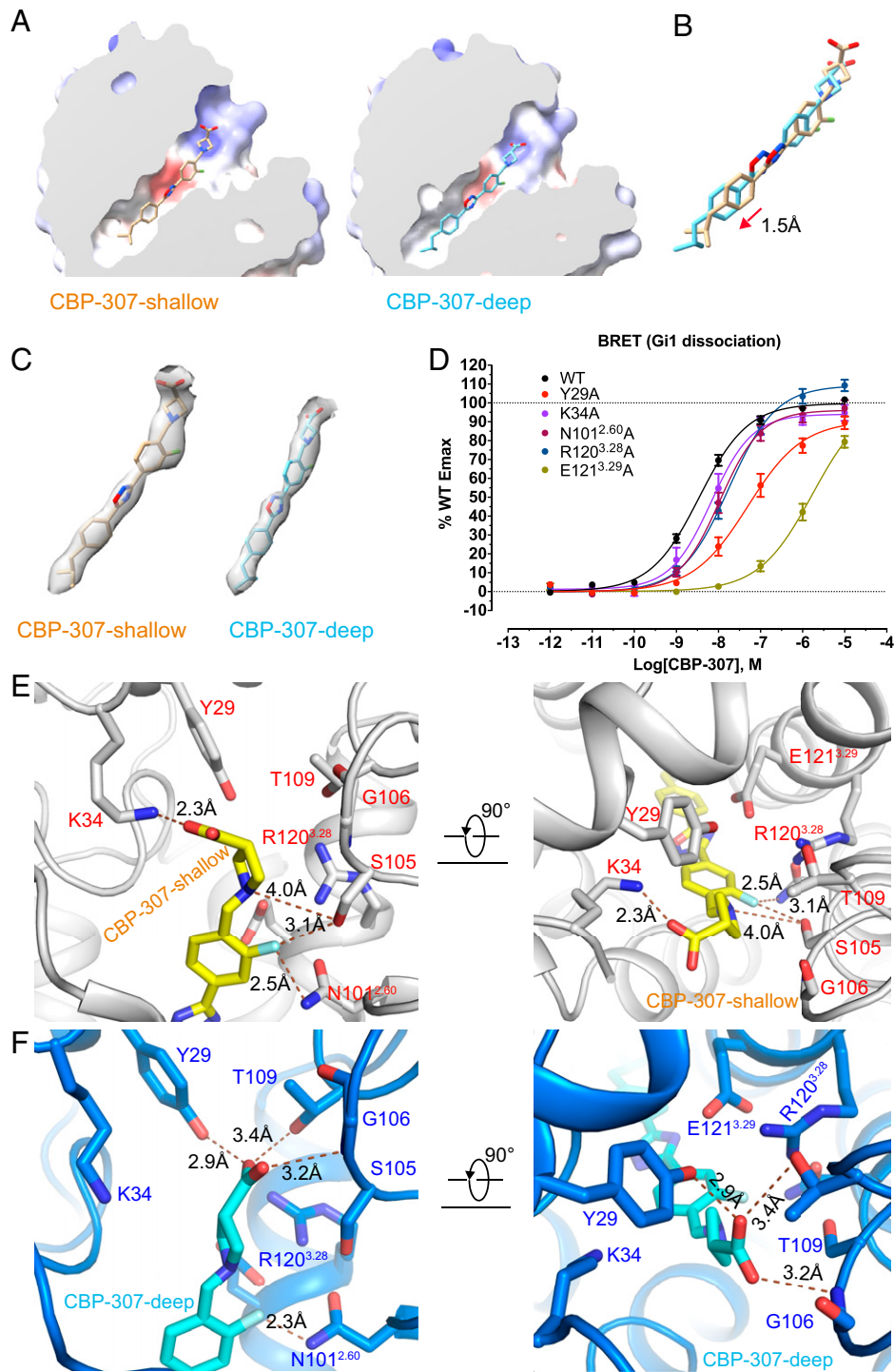


Fig. 4. CBP-307 binding with S1PR1 in two binding modes. (A) A cutaway representation of two binding modes of CBP-307 bound S1PR1 at the level of binding pocket and colored according to surface electrostatic potential with cut surface shown in gray. CBP-307 in shallow mode is colored in wheat. CBP-307 in deep mode is colored in cyan. CBP-307 is shown in sticks. (B) Superposition of two binding modes of CBP-307. CBP-307 in deep mode inserts into the pocket deeper with a 1.5-Å distance than shallow mode. CBP-307 is shown and colored as in A. (C) CBP-307 is modeled in two density maps. (D) The effects of Y29A, K34A, N101^{2,60}A, R120^{3,28}A, and E121^{3,29}A mutations of S1PR1 on CBP-307 induced Gi signal activation measured by Gi dissociation assay (BRET assay). All data are mean \pm SEM of three independent experiments for wild-type or mutants. (E) The key residues interacted with the polar groups of CBP-307 in shallow mode. S1PR1 and CBP-307 are shown in gray and yellow, respectively. CBP307, Y29, K34, N101^{2,60}, S105, G106, T109, R120^{3,28}A, and E121^{3,29}A are shown in sticks. Dashed lines indicate the polar interactions between CBP-307 and K34, N101^{2,60}, and S105 with distances. (F) The key residues interacted with the polar groups of CBP-307 in deep mode. S1PR1 and CBP-307 are shown in marine and cyan, respectively. CBP307, Y29, K34, N101^{2,60}, S105, G106, T109, R120^{3,28}A, and E121^{3,29}A are shown in sticks. Dashed lines with distances indicate the polar interactions between CBP-307 and Y29, N101^{2,60}, G106, and T109.

and the fluorine interacts with N101^{2,60} and S105 due to its negatively charged property (Fig. 4E). Besides, the nitrogen atom of azetidine forms a weak hydrogen bond with S105 (Fig. 4E). In the deep mode, the carboxyl group of CBP-307 forms extensive hydrogen bonds to Y29, G106, and T109 (Fig. 4F).

Additionally, the deeper insertion of CBP-307 makes its nitrogen atom of azetidine closer to E121^{3,29} to form stronger interaction than the shallow mode (*SI Appendix*, Fig. S9). All observations suggest that, in the deep mode, CBP-307 binds to the hydrophilic part of the S1PR1 pocket stronger and similar to the

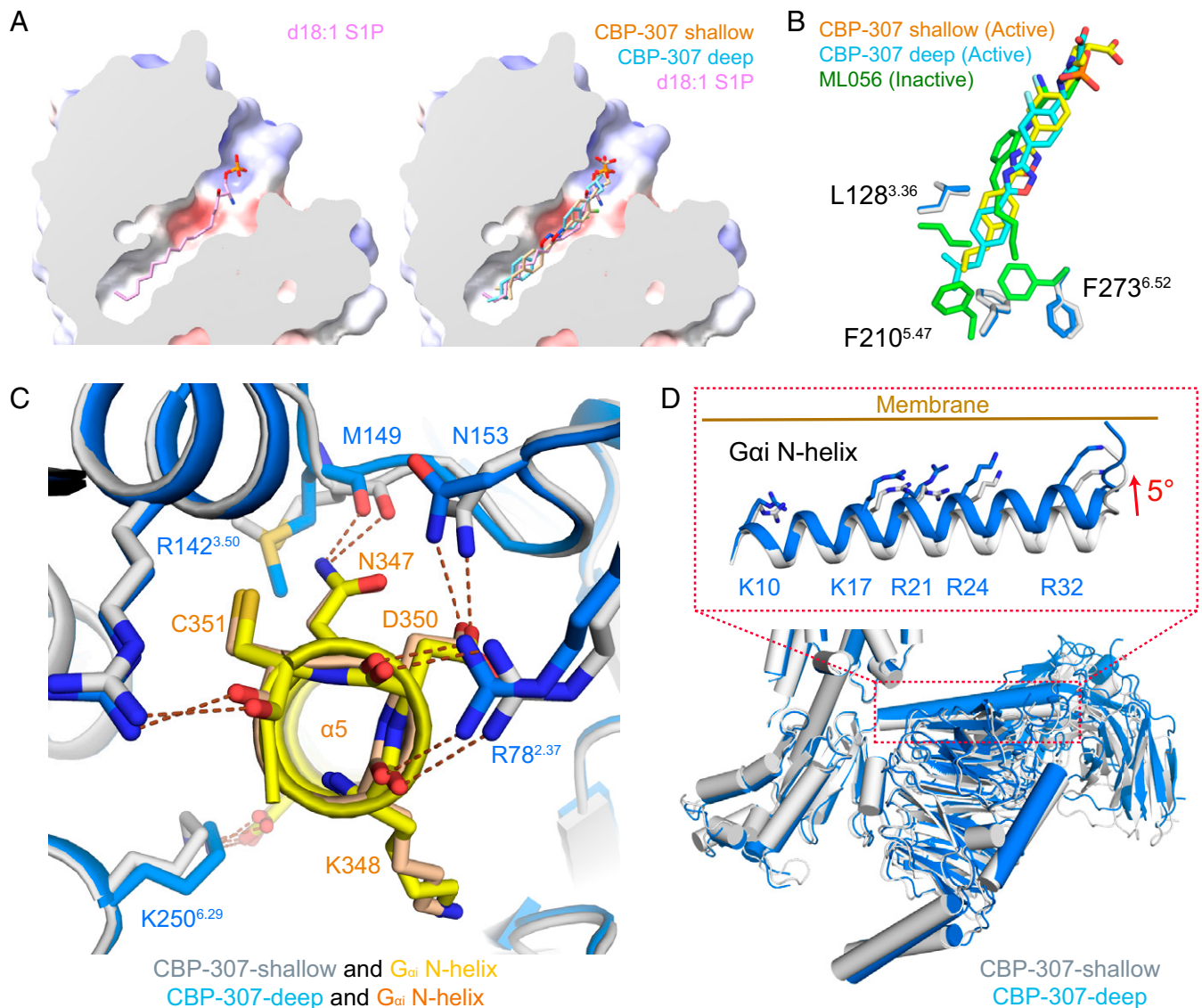


Fig. 5. Activation of S1PR1 by CBP-307. (A) A cutaway representation of d18:1 S1P in the S1PR1-G_i-d18:1 S1P model and superimposed two CBP-307 binding modes with d18:1 S1P in the S1PR1-G_i-d18:1 S1P model. The cutaway surface of S1PR1 with d18:1 S1P is shown at the level of binding pocket and colored according to surface electrostatic potential with cut surface shown in gray. d18:1 S1P and CBP-307 are shown in sticks. d18:1 S1P, CBP-307 (shallow), and CBP-307 (deep) are shown in violet, wheat, and cyan, respectively. (B) Superposition of ML056 with CBP-307-inactive and two CBP-307-bound active forms. ML056, CBP-307-shallow, and CBP-307-deep are shown in sticks colored in green, yellow, and cyan, respectively. Residues near the isobutyl group, including L128^{3.36}, F210^{5.47}, and F273^{6.52} in S1PR1-ML056, S1PR1-CBP-307 (shallow), and S1PR1-CBP-307 (deep), are shown in sticks and colored in green, gray, and marine, respectively. (C) The polar interactions of G_i and S1PR1 with CBP-307 in two modes are similar. S1PR1-CBP-307 (shallow) and S1PR1-CBP-307 (deep) are shown in gray and marine, respectively. The helix 5 of G_{ai} in S1PR1-CBP-307 (shallow) and S1PR1-CBP-307 (deep) are shown in yellow and wheat, respectively. Residues on S1PR1 and helix 5 of G_{ai} are shown in sticks. (D) The N-terminal helix of G_{ai} rich in positive charge residues at a closer position to the membrane in the CBP-307 deep-mode structure. CBP-307 deep and shallow modes are colored in marine and gray, respectively. The positive charge residues (K10, K17, R21, R24, and R32) on the N-terminal helix of G_{ai} are shown in sticks in *D, Inset*.

binding modes of d18:1 S1P and (S)-FTY720-P to the receptor (*SI Appendix, Fig. S9*). Extensive molecular dynamic (MD) simulations were also performed to confirm our speculation further. The result showed that the CBP-307 in the shallow mode inserted deeper after about 20ns and stayed in a similar position to the deep mode for longer than 250ns, consistent with our observations in structures (*SI Appendix, Fig. S10*).

Activation of S1PR1 by CBP-307. In the superposition of d18:1 S1P-bound and two CBP-307-bound structures, the isobutyl group of CBP-307 in the deep binding mode occupies the space of the acyl end of d18:1 S1P, acting as the similar function in S1PR1 activation (Fig. 5A). Notably, the isobutyl group of CBP-307 in the shallow mode has less stereo clash with

F210^{5.47} than in the deep mode, although the receptor is still activated (Fig. 5B). In both binding modes, the interfaces between S1PR1 and the $\alpha 5$ helix of G_{ai} are almost identical. The residues R78^{2.37}, R142^{3.50}, and K250^{6.29} on S1PR1 form hydrogen bonds with the carbonyl oxygen of K348, D345, and C351 and the carboxyl group of D341 on G_{ai}, respectively. The side chains of N153 on ICL2 of S1PR1 and D350 on G_{ai} form a hydrogen bond. The carbonyl oxygen of M149 on ICL2 of S1PR1 interacts with N347 on G_{ai} (Fig. 5C). This extensive hydrogen-bond network forces G_{ai} to bind to S1PR1 tightly.

However, the N-terminal helices of G_{ai} in these two structures have a 5° rotation (Fig. 5D and *SI Appendix, Fig. S11A*). This rotation leads to the following movement of G _{β} and G _{γ} .

The N-terminal helix of $G_{\alpha i}$ is rich in positively charged residues such as K10, K17, R21, R24, and R32 (Fig. 5D). These positively charged residues pointed in the same direction interact with membrane lipids. The N-terminal helix of $G_{\alpha i}$ in the deep model is closer to the membrane and may help to stabilize the S1PR1- G_i complex. Structure alignment also suggested that the overall structure of the CBP-307 deep mode is similar to the structure of the d18:1 S1P-bound S1PR1 complex (SI Appendix, Fig. S11B) and the four structures reported by Shao and colleagues (29) (SI Appendix, Fig. S11C). With the analysis of CBP-307 binding modes and the conformational change of G-protein complexes, we propose a two-step model of S1PR1 activation by CBP-307. Two structures represented two relatively stable conformations during S1PR1 activation. First, CBP-307 binds to the shallow binding site, activates S1PR1, and recruits G_i to form a complex. Then, CBP-307 moves deeper to trigger the G_i complex rotation toward the membrane and further stabilizes the S1PR1- G_i complex. The cell-surface expression levels of all S1PR1 mutants we discussed were carefully evaluated by bioluminescence resonance energy transfer (BRET) assay to ensure that receptors folds properly (SI Appendix, Fig. S12).

Discussion

Although a few structures of inactive S1PR1 and active structures of S1PR1, S1PR3, and S1PR5 were reported, and the selectivity of the alkyl length of S1P analogs was carefully examined (28, 34), it is still valuable to determine the S1P-bound S1PR1 active structure. Moreover, different agonists' recognition and activation of S1PRs need to be studied extensively. Here, we reported G_i -coupled active structures of S1PR1 with three distinct agonists, revealing the agonist recognition and receptor-activation mechanism of S1PR1. The previous MD simulation studies suggested that lipidic agonists may enter the pocket through the cleft between the extracellular half of TM1 and TM7 (35). Residue E121^{3,29} may guide S1P penetration and stabilization, while W269^{6,48} moving toward TM7 results in receptor activation through forming a hydrogen-bond network in the intracellular half of TM7 (36). The space between TM3 and TM6 is increased upon G-protein complex binding. All these speculations were also observed in the active-state structures we reported. Since key residues we identified with composing the orthosteric binding pockets and mediating receptor activation, including Y29, K34, N101^{2,60}, S105, G106, R120^{3,28}, E121^{3,29}, F125^{3,33}, F210^{5,47}, W269^{6,48}, L272^{6,51} (L259^{6,51} in S1PR2), L276^{6,55} (F263^{6,51} in S1PR3), and L297^{7,39} (F274^{7,39} in S1PR2), are almost identical among S1PRs, they would share the very similar activation mechanism upon d18:1 S1P binding.

CBP-307 is currently being evaluated in a global phase 2 clinical study in moderate to severe ulcerative colitis and Crohn's disease (37). As reported, CBP-307 is a specific agonist for S1PR1/4/5 and has significantly higher potency for S1PR1 than for S1PR4 and S1PR5, which is also confirmed by the G_i dissociation assay we performed (SI Appendix, Fig. S13A). The reduction of nonspecific activation of S1PR2 will protect the vascular integrity, and that of S1PR3 may reduce the risk of fibrosis and bronchoconstriction. However, the detailed mechanism of CBP-307 selectivity is still poorly understood. We compared the CBP-307-bound S1PR1- G_i structure (deep mode) to siponimod-bound S1PR5- G_i and the d18:1 S1P-bound S1PR3- G_i structures reported by Shao and colleagues

(29, 30). Residues composed of the orthosteric binding pocket of S1PR1 and S1PR5 are highly conserved (SI Appendix, Fig. S6). Only a few polar residues adopted different rotamers to coordinate the polar head of different agonists (SI Appendix, Fig. S13B). It could explain the cross-activity of CBP-307 to S1PR1 and S1PR5 to some extent. The corresponding residue of L276^{6,55} in S1PR1 is F263^{6,51} in S1PR3. Another two residues in S1PR1, S129^{3,37} and V132^{3,40} (G123 and T126 in S1PR3), are variable (SI Appendix, Fig. S13C). Considering the importance of L276^{6,55} in S1PR1 activation and the locations of S129^{3,37} and V132^{3,40}, further investigation combining structural information, MD simulations, and pharmacological analysis is needed. When we examined the orthosteric binding pocket of S1PR1 with different agonists, two unoccupied subpockets were observed in the d18:1 S1P-bound structure (SI Appendix, Fig. S13D). These two subpockets are different from those identified in S1PR3 (30). More strikingly, the second subpocket is also empty in the other three S1PR1 structures (SI Appendix, Fig. S13E). This pocket can be occupied by agonists to improve the potency and selectivity by designing derivatives of S1PR1 agonists. Collectively, since the structure-based drug design has been applied to many GPCRs, it is vital to obtain structures of S1PRs in multiple conformations bound with diverse ligands to benefit drug-discovery targeting S1PRs by reducing side effects or extending indications.

Materials and Methods

Detailed experimental procedures used in this study, including molecular cloning, cell culture, recombinant protein expression and purification, cryo-EM data collection, and structure determination, are available in SI Appendix, Materials and Methods.

Data Availability. Atomic coordinates and EM density maps of four structures have been deposited in PDB (ID codes 7VIE-7VIH) and the Electron Microscopy Data Bank (accession nos. EMDB-32006-EMDB-32009), respectively. The structure models are presented by PyMOL (<https://pymol.org/2/>), and the density maps are presented by Chimera and Chimera X (38, 39).

ACKNOWLEDGMENTS. We are grateful to Connect Biopharm for donating agonist CBP-307 and for critical discussion. We also thank the Kobilka Cryo-EM Center at the Chinese University of Hong Kong, Shenzhen, for supporting EM data collection. This work was supported by National Natural Science Foundation of China Projects 31971218 (to R.R.), 32071197 (to S.W.), and 31971179 (to L.Z.); the Ministry of Science and Technology of China (2020YFA0509102 to S.W.); Science, Technology, and Innovation Commission of Shenzhen Municipality Projects JCYJ-20180307-151618765 and JCYJ-20180508-163206306 (to R.R.) and JCYJ-2020010915-0003938 and RCYX20200714114645019 (to L.Z.); the Shanghai Science and Technology Committee (19ZR1466200 to S.W.); and the Thousand Talents Plan-Youth and Shanghai Rising-Star Program (20QA1410600 to S.W.). R.R. and L.Z. were also supported in part by a Presidential Fellowship, and B.G. and R.T. were supported by a Ganghong Youth Scholarship at the Chinese University of Hong Kong, Shenzhen.

Author affiliations: ^aKobilka Institute of Innovative Drug Discovery, School of Life and Health Sciences, The Chinese University of Hong Kong, Shenzhen 518172, China; ^bShanghai Key Laboratory of Metabolic Remodeling and Health, Institute of Metabolism and Integrative Biology, Fudan University, Shanghai 200437, China; ^cSchool of Life Sciences, University of Science and Technology of China, Anhui 230026, China; ^dState Key Laboratory of Molecular Biology, Shanghai Institute of Biochemistry and Cell Biology, Center for Excellence in Molecular Cell Science, University of Chinese Academy of Sciences, Chinese Academy of Sciences, Shanghai 200031, China; ^eWarshal Institute of Computational Biology, School of Life and Health Sciences, The Chinese University of Hong Kong, Shenzhen 518172, China; ^fZhangjiang Laboratory, National Facility for Protein Science in Shanghai, Shanghai Advanced Research Institute, Chinese Academy of Sciences, Shanghai 201210, China; and ^gSuzhou Connect Biopharmaceuticals, Ltd

1. Anonymous, Treatise on the chemical constitution of the brain: Based throughout upon original researches. *Glasg. Med. J.* **22**, 363–364 (1884).
2. S. Spiegel, S. Milstien, Sphingosine-1-phosphate: An enigmatic signalling lipid. *Nat. Rev. Mol. Cell Biol.* **4**, 397–407 (2003).
3. J. Chun, H.-P. Hartung, Mechanism of action of oral fingolimod (FTY720) in multiple sclerosis. *Clin. Neuropharmacol.* **33**, 91–101 (2010).
4. H. Liu *et al.*, Molecular cloning and functional characterization of a novel mammalian sphingosine kinase type 2 isoform. *J. Biol. Chem.* **275**, 19513–19520 (2000).
5. S. el Bawab, C. Mao, L. M. Obeid, Y. A. Hannun, Ceramidases in the regulation of ceramide levels and function. *Subcell. Biochem.* **36**, 187–205 (2002).
6. S. Fukuhara *et al.*, The sphingosine-1-phosphate transporter Spns2 expressed on endothelial cells regulates lymphocyte trafficking in mice. *J. Clin. Invest.* **122**, 1416–1426 (2012).
7. R. Ren, B. Pang, Y. Han, Y. Li, A glimpse of the structural biology of the metabolism of sphingosine-1-phosphate. *Contact* **4**, 2515256421995601 (2021).
8. E. J. Goetzl, Y. Kong, B. Mei, Lysophosphatidic acid and sphingosine 1-phosphate protection of T cells from apoptosis in association with suppression of Bax. *J. Immunol.* **162**, 2049–2056 (1999).
9. G. Dorsam, M. H. Graeler, C. Serogy, Y. Kong, J. K. Voice, E. J. Goetzl, Transduction of multiple effects of sphingosine 1-phosphate (S1P) on T cell functions by the S1P1 G protein-coupled receptor. *J. Immunol.* **171**, 3500–3507 (2003).
10. C. Watson *et al.*, High expression of sphingosine 1-phosphate receptors, S1P1 and S1P3, sphingosine kinase 1, and extracellular signal-regulated kinase-1/2 is associated with development of tamoxifen resistance in estrogen receptor-positive breast cancer patients. *Am. J. Pathol.* **177**, 2205–2215 (2010).
11. H. A. Neubauer *et al.*, An oncogenic role for sphingosine kinase 2. *Oncotarget* **7**, 64886–64899 (2016).
12. Y. Liu *et al.*, Edg-1, the G protein-coupled receptor for sphingosine-1-phosphate, is essential for vascular maturation. *J. Clin. Invest.* **106**, 951–961 (2000).
13. D. J. Baek *et al.*, Structure-activity relationships and molecular modeling of sphingosine kinase inhibitors. *J. Med. Chem.* **56**, 9310–9327 (2013).
14. J. T. Bagdanoff *et al.*, Inhibition of sphingosine-1-phosphate lyase for the treatment of autoimmune disorders. *J. Med. Chem.* **52**, 3941–3953 (2009).
15. A. Billich, C. Beerli, R. Bergmann, C. Bruns, E. Loetscher, Cellular assay for the characterization of sphingosine-1-phosphate lyase inhibitors. *Anal. Biochem.* **434**, 247–253 (2013).
16. A. Nitzsche *et al.*, Endothelial S1P₁ signaling counteracts infarct expansion in ischemic stroke. *Circ. Res.* **128**, 363–382 (2021).
17. A. Koch, J. Pfeilschifter, A. Huwiler, Sphingosine 1-phosphate in renal diseases. *Cell. Physiol. Biochem.* **31**, 745–760 (2013).
18. R. L. Proia, T. Hla, Emerging biology of sphingosine-1-phosphate: Its role in pathogenesis and therapy. *J. Clin. Invest.* **125**, 1379–1387 (2015).
19. E. Melamed, M. W. Lee, Multiple sclerosis and cancer: The ying-yang effect of disease modifying therapies. *Front. Immunol.* **10**, 2954 (2020).
20. E. Jozefczuk, T. J. Guzik, M. Siedlinski, Significance of sphingosine-1-phosphate in cardiovascular physiology and pathology. *Pharmacol. Res.* **156**, 104793 (2020).
21. B. Zemann *et al.*, Sphingosine kinase type 2 is essential for lymphopenia induced by the immunomodulatory drug FTY720. *Blood* **107**, 1454–1458 (2006).
22. S. Pan *et al.*, Discovery of BAF312 (Siponimod), a potent and selective S1P receptor modulator. *ACS Med. Chem. Lett.* **4**, 333–337 (2013).
23. F. L. Scott *et al.*, Ozanimod (RPC1063) is a potent sphingosine-1-phosphate receptor-1 (S1P1) and receptor-5 (S1P5) agonist with autoimmune disease-modifying activity. *Br. J. Pharmacol.* **173**, 1778–1792 (2016).
24. V. Brinkmann, FTY720 (fingolimod) in multiple sclerosis: Therapeutic effects in the immune and the central nervous system. *Br. J. Pharmacol.* **158**, 1173–1182 (2009).
25. M. Fronza, L. Lorefice, J. Frau, E. Cocco, An overview of the efficacy and safety of ozanimod for the treatment of relapsing multiple sclerosis. *Drug Des. Devel. Ther.* **15**, 1993–2004 (2021).
26. T. Brummer, T. Ruck, S. G. Meuth, F. Zipp, S. Bittner, Treatment approaches to patients with multiple sclerosis and coexisting autoimmune disorders. *Ther. Adv. Neurol. Disord.* **14**, 17562864211035542 (2021).
27. M. A. Hanson *et al.*, Crystal structure of a lipid G protein-coupled receptor. *Science* **335**, 851–855 (2012).
28. S. Maeda *et al.*, Endogenous agonist-bound S1PR3 structure reveals determinants of G protein-subtype bias. *Sci. Adv.* **7**, eabf5325 (2021).
29. Y. Yuan *et al.*, Structures of signaling complexes of lipid receptors S1PR1 and S1PR5 reveal mechanisms of activation and drug recognition. *Cell Res.* **31**, 1263–1274 (2021).
30. C. Zhao *et al.*, Structural insights into sphingosine-1-phosphate recognition and ligand selectivity of S1PR3-Gi signaling complexes. *Cell Res.* **32**, 218–221 (2022).
31. J. A. R. Dalton, I. Lans, J. Giraldo, Quantifying conformational changes in GPCRs: Glimpse of a common functional mechanism. *BMC Bioinformatics* **16**, 124 (2015).
32. K. Krishna Kumar *et al.*, Structure of a signaling cannabinoid receptor 1-G protein complex. *Cell* **176**, 448–458 (2019).
33. L. Wang *et al.*, Structures of the human PGD₂ receptor CRTH2 reveal novel mechanisms for ligand recognition. *Mol. Cell* **72**, 48–59 (2018).
34. A. Trounion-Tsailaki *et al.*, Ligand chain length drives activation of lipid G protein-coupled receptors. *Sci. Rep.* **7**, 2020 (2017).
35. A. D. Caliman, Y. Miao, J. A. McCammon, Activation mechanisms of the first sphingosine-1-phosphate receptor. *Protein Sci.* **26**, 1150–1160 (2017).
36. Z. Jiang, H. Zhang, Molecular mechanism of S1P binding and activation of the S1P₁ receptor. *J. Chem. Inf. Model.* **59**, 4402–4412 (2019).
37. A. J. Dyckman, Modulators of sphingosine-1-phosphate pathway biology: Recent advances of sphingosine-1-phosphate receptor 1 (S1P₁) agonists and future perspectives. *J. Med. Chem.* **60**, 5267–5289 (2017).
38. E. F. Pettersen *et al.*, UCSF Chimera—A visualization system for exploratory research and analysis. *J. Comput. Chem.* **25**, 1605–1612 (2004).
39. E. F. Pettersen *et al.*, UCSF ChimeraX: Structure visualization for researchers, educators, and developers. *Protein Sci.* **30**, 70–82 (2021).